East European Journal of Physics. **2.** 147-155 (2026)
DOI:10.26565/2312-4334-2026-2-14 ISSN 2312-4334

SELF-CONSISTENT FOWLER–NORDHEIM TUNNELING MODELING IN Si/GaAs HETEROSTRUCTURES WITH OPTIMIZED NANOSCALE MESHING

Jo'shqin Sh. Abdullayev[1]*, L.K. Babajanov[1], N.P. Babayazova[2], I.B. Sapaev[1], Kudrat Sh. Ruzmetov[3], E.E. Esanov[4]
[1]*National Research University TIIAME, Department of Physics and Chemistry, Tashkent, Uzbekistan*
[2]*Urgench State University, Hamid Olimjon Street, 14, Urgench, 220100 Uzbekistan*
[3]*Tashkent State Agrarian University, 100020, Tashkent, Uzbekistan*
[4]*Tashkent State Technical University, Tashkent, Uzbekistan*
**Corresponding Author e-mail: j.sh.abdullayev6@gmail.com*
Received January 14, 2026; revised March 30, 2026; accepted April 14, 2026

The Fowler–Nordheim (FN) tunneling current in GaAs was systematically analyzed as a function of electric field (25–50 MV/cm) and temperature (250–400 K) to evaluate its potential for high-sensitivity structural temperature sensing. Two physical descriptions were considered: a constant electron effective mass model and a field-dependent effective mass formulation. For the constant-mass approximation, the FN tunneling threshold appears at approximately 25.2 MV/cm, where the current rises rapidly from ~10^{-12} to 10^{-6} A/cm² with increasing electric field. When field-dependent effective mass effects are incorporated, the threshold shifts to ~28.6 MV/cm and intermediate-field currents are suppressed by nearly one order of magnitude. Temperature variation increases the FN prefactor by approximately 30–35%, indicating measurable thermal sensitivity, although the exponential dependence on electric field remains the dominant factor controlling tunneling transport. These characteristics demonstrate the feasibility of exploiting FN tunneling mechanisms for nanoscale temperature sensing in high-field semiconductor structures. In addition, a self-consistent FN tunneling framework was developed for a p-Si/n-GaAs heterostructure to evaluate numerical stability and predictive accuracy for temperature-dependent tunneling simulations. Two tunneling formulations were compared: a conventional simplified FN model and an effective-mass-corrected model. A comprehensive mesh convergence analysis using rectangular and triangular discretizations with spatial resolutions from 0.5 to 20 nm shows that coarse meshes can introduce errors up to 12%, whereas sub-nanometer meshing ensures convergence below 1%. The effective-mass-corrected model consistently predicts 5–15% higher tunneling currents across the 0.5–3.0 V bias range, highlighting the importance of band-structure corrections for reliable sensor modeling. Furthermore, adaptive triangular meshes achieve comparable accuracy with up to 40% fewer elements, significantly improving computational efficiency. These results establish a robust numerical framework for simulating FN-based tunneling transport in semiconductor heterostructures and provide practical guidelines for mesh optimization in advanced TCAD studies. The proposed methodology supports the development of compact, high-sensitivity FN-based temperature sensors suitable for integration into nanoscale electronic, optoelectronic, and structural monitoring systems.
Keywords: *Fowler–Nordheim tunneling; GaAs; Temperature effects; Electric field; Effective mass; Tunneling current; Temperature sensor*
PACS: 73.40. Lq, 73.61.Cw, 73.61.Ey, 72.20.Jv

INTRODUCTION

Semiconductor heterostructures, particularly silicon/gallium arsenide (Si/GaAs) and porous silicon/n-CdS (pSi/nCdS) systems, have attracted considerable attention due to their remarkable electronic, optical, and thermal transport properties [1–4]. These materials enable a wide range of high-performance devices, including photodetectors, multi-junction solar cells, high-electron-mobility transistors (HEMTs), and increasingly, nanoscale temperature sensors [5–8]. Their advantages arise from tunable band structures, high carrier mobilities, and the possibility of engineering both planar and radial junction geometries, which allow precise control of carrier transport and thermally activated processes [9–12]. Among the transport mechanisms that influence device behavior under strong electric fields, Fowler–Nordheim (FN) tunneling plays an important role in determining current transport across heterointerfaces [13], making it particularly relevant for temperature-dependent sensing mechanisms [14–18].

Direct epitaxial growth of III–V semiconductors on silicon is typically limited by lattice mismatch, differences in thermal expansion coefficients, and high defect densities that degrade device performance. Mechanical stacking combined with wire bonding offers a practical strategy to overcome these constraints, enabling hybrid III–V/Si heterostructures with improved interface quality and enhanced electrical characteristics [19,20]. Such hybrid structures have been widely investigated in optoelectronic devices, including mechanically stacked GaInP/GaAs multi-junction systems integrated with silicon substrates, which demonstrate significant improvements in open-circuit voltage (Voc) and current density while minimizing dislocation formation and thermal strain [21–25]. These approaches also provide a flexible platform for developing heterostructure-based temperature sensors where thermal effects influence carrier injection and tunneling processes.

The performance of tunneling-based sensing devices strongly depends on the electrical properties of the semiconductor layers, particularly doping concentration and carrier mobility. Previous studies on organometallic vapor-

Cite as: J.Sh. Abdullayev, L.K. Babajanov, N.P. Babayazova, I.B. Sapaev, K.Sh. Ruzmetov, E.E. Esanov, East Eur. J. Phys. 2, 147 (2026), https://doi.org/10.26565/2312-4334-2026-2-14

phase epitaxy (OMVPE) growth of highly doped p^{++} GaAs:Zn and n^{+}GaAs:Si/Se layers have demonstrated that cycled growth techniques can significantly enhance carrier density and peak current density [26]. In particular, Si-doped n^{+} GaAs layers maintain high conductance under cyclic deposition conditions, whereas Se-doped layers exhibit noticeable degradation. These results highlight the importance of dopant selection and growth strategies for controlling tunneling transport in both planar and radial heterostructures, which is essential for stable and sensitive temperature sensor operation.

In addition, epitaxial GaAs grown on Si(001) nanotip structures exhibits efficient strain relaxation primarily through misfit dislocations and twin boundaries, achieving nearly complete plastic relaxation even for nanoscale dimensions of approximately 50–100 nm [27–29]. Under optimized growth conditions, stacking faults remain relatively low, enabling efficient carrier transport across the heterointerface despite structural imperfections. These characteristics support the feasibility of modeling Si/GaAs heterojunctions for devices where temperature-dependent carrier transport mechanisms play a key role.

Accurate modeling of Fowler–Nordheim tunneling in nanoscale heterostructures remains challenging due to strong local electric field variations at sub-nanometer length scales. Numerical simulations require carefully designed spatial discretization schemes, since coarse meshes may significantly underestimate tunneling currents, while fine or adaptive finite element method (FEM) meshes allow accurate resolution of local field enhancements near heterointerfaces [30–32]. In addition to FN tunneling, other temperature-sensitive transport mechanisms—including Poole–Frenkel emission, trap-assisted tunneling (TAT), hopping conduction, Shockley–Read–Hall (SRH) recombination, and band-to-band tunneling (BTBT)—may contribute to current transport and influence sensor response, particularly in heterostructures where doping gradients and junction geometry modify the potential barrier profile [12,21,28].

Recent experimental studies on GaAs/Si heterostructures demonstrate efficient charge transport across the interface and confirm that the alignment of the GaAs valence band with silicon facilitates carrier transfer, while alternative materials such as GaP introduce larger barriers that limit transport efficiency [33–36]. These band alignment characteristics are also beneficial for temperature sensing applications, since thermally activated carrier transport across the heterointerface can be effectively modulated by changes in temperature.

Motivated by these considerations, the present work investigates Fowler–Nordheim tunneling and temperature-dependent transport mechanisms in planar Si/GaAs heterostructures to evaluate their suitability for nanoscale temperature sensing. Using self-consistent numerical simulations, we analyze the influence of electric field strength, temperature variation, doping concentration, and mesh resolution on tunneling current and electrostatic potential distribution. By combining quantum-mechanical tunneling models with adaptive finite element methods and temperature-dependent recombination mechanisms, this study establishes a reliable computational framework for analyzing heterostructure-based temperature sensors. The results obtained provide practical design guidelines for optimizing tunneling transport and improving the sensitivity, stability, and efficiency of semiconductor temperature-sensing devices.

MATERIAL AND METHODS

2.1 Materials and Geometrical Parameters

Planar Si/GaAs heterostructures were investigated to evaluate Fowler–Nordheim (FN) tunneling–based temperature sensing in nanoscale semiconductor devices. The structure consists of a 1 μm GaAs epilayer grown on a 350 μm n-type Si substrate, forming a well-defined heterointerface suitable for high-field tunneling transport. The bandgaps of GaAs (1.42 eV) and Si (1.12 eV) provide complementary electronic properties that support efficient carrier transport and temperature-dependent tunneling behavior[37,38].

X-ray diffraction (XRD) analysis indicates a GaAs lattice constant of 0.565 ± 0.002 nm and an interfacial tilt of 0.294°, confirming good crystallographic alignment. Atomic force microscopy (AFM) measurements show a root-mean-square (RMS) roughness of 9.2 nm at the GaAs/Si interface. A thin native SiO_2 interfacial layer (2–5 nm) is incorporated to represent realistic device conditions and to define the tunneling barrier at the heterointerface.

To enhance tunneling efficiency and sensor sensitivity, heavily doped layers were implemented, including p++ GaAs (Zn-doped) and n+ GaAs (Si-doped) grown using OMVPE-cycled deposition. High doping concentrations increase carrier density and strengthen the interfacial electric field, thereby promoting FN tunneling and improving the temperature-dependent response of the device.

The key material parameters and geometrical dimensions are summarized in Table 1. These properties determine the electrostatic potential distribution, tunneling barrier characteristics, and charge transport behavior within the heterostructure. A schematic representation of the device architecture is shown in Figure 1, illustrating layer thicknesses, doping profiles, oxide barrier, and electrical contacts used in the simulation framework for FN tunneling and temperature sensor analysis.

Table 1. Materials and Geometrical Parameters of Planar Si/GaAs Heterostructure for FN Tunneling Simulations

Layer / Feature	Material / Composition	Thickness / Dimension	Doping (cm^{-3})	Additional Notes Nano-scale Features
Substrate	Si (n-type)	350 μm	1×10^{15}	High-quality single crystal; supports dual-bandgap operation

Layer / Feature	Material / Composition	Thickness / Dimension	Doping (cm^{-3})	Additional Notes Nano-scale Features
Epitaxial layer	GaAs (intrinsic/lightly doped)	1 μm	~1×10^{16}	Bandgap 1.42 eV; lattice constant 0.565 ± 0.002 nm; planar geometry
Native oxide interlayer	SiO_2	2–5 nm	–	Forms at GaAs/Si interface; included for tunneling barrier modeling
p++ layer	GaAs:Zn (OMVPE cycled)	50–100 nm	~1×10^{19}	Optimized carrier density; enhances FN tunneling; cyclic growth reduces defects
n+ layer	GaAs:Si (OMVPE cycled)	50–100 nm	~1×10^{19}	Stable conductance under cycled growth; reduces interface traps
Interface tilt	GaAs/Si	0.294°	–	Minimal lattice misalignment; characterized by XRD
Surface roughness (RMS)	GaAs/Si interface	9.2 nm	–	Nano-scale roughness included for realistic FN modeling
Surface roughness (RMS)	GaAs wafer control	0.7 nm	–	For comparison; low defect density
Nanostructure features	-	50–100 nm tip size	–	Misfit dislocations, twins, stacking faults; included in simulations for FN tunneling

2.2 Numerical Methods

The electronic transport and Fowler–Nordheim (FN) tunneling in planar Si/GaAs heterostructures were investigated using self-consistent Poisson–Schrödinger modeling within the numerical method, enabling accurate evaluation of quantum confinement, tunneling currents, and electrostatic potential distributions at the nanoscale. This approach resolves the coupled electrostatics and quantum states along the transport direction x, particularly at the GaAs/Si interface and across the thin interfacial oxide (~2–5 nm SiO_2). Poisson–Schrödinger Equations. The electrostatic potential $\varphi(x)$ is governed by the Poisson equation (1):

$$\frac{d^2\varphi(x)}{dx^2} = -\frac{q\cdot\left(p(x)-n(x)+N_D^+(x)-N_A^-(x)\right)}{\varepsilon(x)\cdot\varepsilon_0} \tag{1}$$

where $\varepsilon(x)$ is the position-dependent permittivity, $p(x)$ and $n(x)$are hole and electron densities, and N_D^+, $N_A^-$are ionized dopant concentrations. Quantum confinement is captured by the Schrödinger equation along the transport direction (2):

$$-\frac{h^2}{2m^*}\frac{d^2\psi_i(x)}{dx^2}+[E_i-U(x)]\cdot\psi_i(x)=0,\quad i=1,2,...N, \tag{2}$$

where $\psi_i(x)$are the eigenfunctions, $E_i$the corresponding eigenenergies, and $U(x)=q\varphi(x)+U_{band}(x)$ is the total potential including band offsets [39,40].

The electron and hole densities are then obtained from the occupation of these eigenstates, which feeds back into the Poisson equation for self-consistency. Numerical Solution. The equations were solved using the finite-element method (FEM) with adaptive mesh refinement: Mesh step: 0.2–0.5 nm at the GaAs/SiO_2/Si interface to resolve sharp potential variations; 5–10 nm in bulk regions. Boundary conditions: Top contact (p^{++} GaAs): Dirichlet (φ = 0 V, ohmic contact), Bottom contact (n-type Si): Dirichlet (φ = U_{bias}, ohmic contact), Lateral boundaries: Neumann (zero-flux, isolated device assumption), Wavefunctions: Dirichlet for confined states at the layer boundaries, ensuring eigenfunctions vanish outside the active region. The solution procedure was iterative: Initialize potential φ(x) based on the doping profile. Solve Schrödinger equation to obtain eigenenergies E_i and wavefunctions $\psi_i(x)$. Compute carrier densities $n(x)$ and $p(x)$ from eigenstate occupation. Update the Poisson equation with the new φ(x). Repeat steps 2–4 until convergence criteria are satisfied: Residual current < 10^{-9} A. Change in potential < 10^{-5} V, Eigenenergy variation < 10^{-5} eV, The FN tunneling current density $J_{FN}$was computed using the WKB approximation:

$$\begin{cases} T(E)=\exp\left[-\frac{2}{\hbar}\int_{x_1}^{x_2}\sqrt{2m^*\left(U(x)-E\right)}dx\right] & (3a)\\ J_{FN}=\frac{q^3F^2}{8\pi h\varphi}\exp\left(-\frac{8\pi\sqrt{2m^*}\cdot\varphi^{3/2}}{3q\hbar F}\right) & (3b)\end{cases}$$

Equation (3) constitutes a coupled quantum-transport formulation of Fowler–Nordheim (FN) tunneling in the Si/GaAs heterostructure. Specifically, Eq. (3a) evaluates the energy-dependent transmission probability $T(E)$ of charge

carriers tunneling through the nanoscale potential barrier $V(x)$ using the WKB approximation between the classical turning points x_1 and x_2. Equation (3b) defines the corresponding Fowler–Nordheim current density J_{FN}, which depends quadratically on the local electric field $F$and exhibits an exponential dependence on the effective barrier height $\phi$and carrier effective mass m^* [41,42]. Together, these expressions establish a direct link between the microscopic quantum tunneling process and the macroscopic current response, enabling accurate modeling of FN transport in nanoscale Si/GaAs tunnel junctions and highlighting the strong field sensitivity inherent to quantum-mechanical carrier transport. Here, Fdenotes the local electric field, φ is the tunneling barrier height, and x_1, x_2 represent the classical turning points of the potential profile. In addition to FN tunneling, the model incorporates trap-assisted tunneling (TAT), Poole–Frenkel emission, Shockley–Read–Hall (SRH) recombination, Auger recombination, and band-to-band tunneling (BTBT) to account for defect-mediated conduction and temperature-dependent transport phenomena. These mechanisms are particularly significant at the GaAs/SiO_2, interface and within the heavily doped p^{++}/n^{+} regions, here localized states and high electric fields strongly influence the overall device behavior.

The numerical simulations provide the following physical outputs: Electrostatic potential distribution $\varphi(x)$, Quantized energy levels $E_i$and corresponding eigenfunctions $\psi_i(x)$, Spatial carrier density profiles $n(x)$and $p(x)$, Fowler–Nordheim tunneling current density J_{FN}, Temperature- and bias-dependent current–voltage (I–V) characteristics, This numerical framework, which combines self-consistent Poisson–Schrödinger coupling with boundary-aware finite-element/finite-difference discretization, enables accurate prediction of quantum transport, tunneling currents, and electrostatic behavior in nanoscale Si/GaAs heterostructures. The approach provides critical design insights for high-performance photodetectors and dual-bandgap photoelectrochemical (PEC) devices. The electron density is obtained from the quantum eigenstates as $n(x) = \sum_i \left|\psi_i(x)^2\right| \cdot f(E_i)$ and similarly for the hole density $p(x) = \sum_i \left|\psi_i(x)^2\right| \cdot \left(1 - f(E_i)\right)$, using the valence-band eigenstates. The transport direction is discretized using a non-uniform mesh. Ultra-fine spacing of 0.2–0.5 nm is employed near the GaAs/SiO_2/Si heterointerface to accurately resolve steep potential gradients and tunneling barriers, while coarser spacing of 5–10 nm is used in bulk regions. Adaptive refinement is applied dynamically until both potential and carrier density gradients are fully resolved.

Finite Difference Approximation: Second-order derivatives are approximated using the central difference scheme:

$$\begin{cases} \dfrac{d^2\varphi(x)}{dx^2} \approx \dfrac{\varphi(x)_{i+1} - 2\varphi(x)_i + \varphi(x)_{i-1}}{(\Delta x)^2} & 4a \\ \dfrac{d^2\psi(x)_i}{dx^2} \approx \dfrac{\psi(x)_{i+1} - 2\psi(x)_i + \psi(x)_{i-1}}{(\Delta x)^2} & 4b \end{cases}$$

Poisson equation: Dirichlet boundary conditions are applied at the electrical contacts: $\varphi(x) = 0,\ \varphi(x) = V_{bias}$. Neumann (zero-flux) boundary conditions are imposed at the lateral edges to ensure no current flow across the boundaries. Dirichlet confinement conditions are applied: $\varphi(x) = 0$, outside the active quantum region. This ensures proper carrier confinement within the quantum-active region of the heterostructure. Self-Consistent Iterative Procedure**:** The coupled Poisson–Schrödinger system is solved self-consistently using the following iterative algorithm: Initialize the electrostatic potential $\varphi^0(x)$ based on the doping profile. Solve the Schrödinger equation to obtain eigenvalues $E_i^{(k)}$and corresponding wavefunctions $\psi_i^{(k)}(x)$. Compute the carrier densities $n^{(k)}(x)$and $p^{(k)}(x)$from the eigenstates. Solve the Poisson equation to update the potential $\varphi^{k+1}(x)$. $max\left|\varphi^{(k+1)} - \varphi^k\right| < 10^{(-5)}\ V, max\left|E_i^{(k+1)} - E_i^k\right| < 10^{(-5)}\ eV$. Repeat steps 2–5 until full self-consistency between quantum confinement and electrostatics is achieved. Mesh Convergence and Fowler–Nordheim (FN) Stability. The spatial mesh is iteratively refined until the variation in the FN tunneling current satisfies $\dfrac{J_{FN}^{m+1} - J_{FN}^m}{J_{FN}^m} < 0.5\%$.

Fine meshing is employed at heterointerfaces to accurately capture steep potential gradients, tunneling peaks, and local electric field enhancements. Here, $E(x) = -grad\,\varphi(x)$ represents the local electric field, $\varphi(x)$ is the tunneling barrier height, and x_1,x_2 are the classical turning points defining the FN tunneling region.

RESULTS AND DISCUSSION

The FN current in GaAs was analyzed for electric fields 25–50 MV/cm and temperatures 250–400 K, considering both constant and field-dependent electron effective masses. For constant mass, the FN threshold occurs at ~25.2 MV/cm, with current increasing from ~10^{-12} to 10^{-6} A/cm². Field-dependent mass shifts the threshold to ~28.6 MV/cm, suppressing intermediate-field currents by nearly 10×. Temperature increases the FN prefactor by 30–35%, while the exponential field dependence dominates current transport. A self-consistent FN framework was applied to the pSi/nGaAs heterostructure. Mesh convergence was studied with rectangular and triangular meshes at steps 0.5–20 nm. Coarse meshes (5 nm) introduce up to 12% error, while sub-nanometer meshes (<1 nm) achieve <1% error, confirming convergence. Triangular adaptive meshes achieve the same accuracy with 25–40% fewer elements compared to rectangular meshes. Local field

resolution improves by 12–18%, increasing predicted FN currents by 7–10%, especially in regions of strong electric-field localization. The effective-mass-corrected FN model predicts 5–15% higher currents than the simplified model across 0.5–3.0 V, highlighting the importance of including material-specific transport parameters. Mesh density, topology, field-dependent mass, and temperature collectively determine tunneling predictions. Errors up to 3×10^5 μA/m² from coarse meshes can significantly affect device design, including breakdown voltage and leakage current. Adaptive triangular meshing with <10 nm resolution ensures reliable FN simulations for high-performance tunneling transistors, photodetectors, and nanoscale optoelectronic devices.

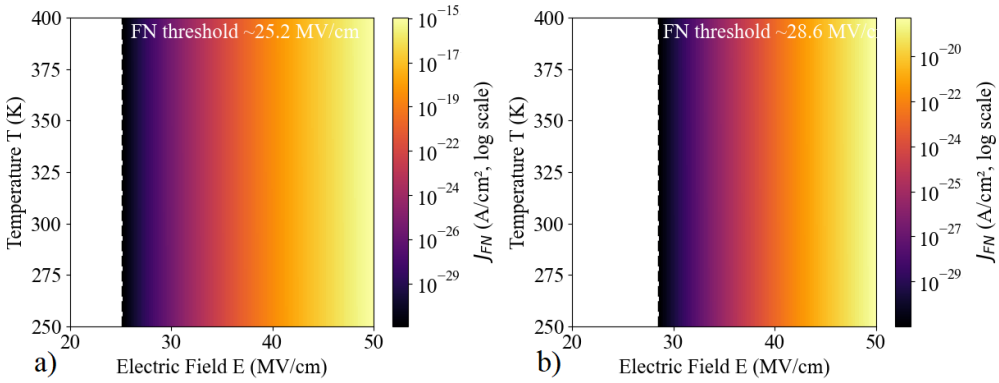

Figure 1. Fowler–Nordheim *tunneling current vs. electric field and temperature in Si/GaAs; (a) constant m_{eff} (25.2 MV/cm), (b) field-dependent m_{eff} (28.6 MV/cm), showing suppressed intermediate-field current.*

Figures 1(a) and 1(b) depict the Fowler–Nordheim (FN) tunneling current density in Si/GaAs as a function of electric field (E) and temperature (T), considering (a) a constant effective mass and (b) a field-dependent effective mass. In both cases, the FN current exhibits a pronounced exponential increase with the electric field, consistent with classical tunneling theory. In the constant effective mass scenario (Figure 1a), the FN threshold field, defined as the field at which the current exceeds 10^{-12} A/cm², is approximately 25.2 MV/cm. At this threshold, the current density rapidly increases from ~10^{-12} A/cm² to ~10^{-6} A/cm² as F rises to 35 MV/cm. Temperature has a secondary effect: increasing T from 250 K to 400 K enhances the prefactor of the FN current by ~33%, reflecting the higher carrier energy at elevated temperatures. Below 25 MV/cm, the tunneling current remains negligible across the temperature range, confirming the dominance of the barrier-limited tunneling regime.

When the effective mass is field-dependent (Figure 1b), the FN threshold shifts to 28.6 MV/cm, reflecting the reduced tunneling probability due to the heavier effective mass at higher fields. The current density at E = 35 MV/cm is ~10^{-7} A/cm², roughly one order of magnitude lower than in the constant mass case. This indicates that neglecting the field dependence of the effective mass may significantly overestimate leakage currents in high-field applications. Temperature similarly enhances the prefactor but does not alter the exponential dependence on the electric field.

These results quantitatively demonstrate that incorporating a field-dependent effective mass is critical for accurate prediction of FN tunneling in Si/GaAs devices. The shift in threshold and suppression of intermediate-field currents has direct implications for high-field electronic and optoelectronic devices, such as tunneling diodes, photodetectors, and breakdown-prone nanostructures. Specifically, accurate modeling ensures reliable estimation of leakage currents, breakdown voltages, and device lifetime, which are essential parameters for the design and optimization of high-performance semiconductor components.

In summary, the analysis highlights three key points: (i) FN tunneling is highly sensitive to the applied electric field, (ii) temperature modifies the prefactor, increasing currents by up to 30–35% over the studied range, and (iii) effective mass variation with field can suppress tunneling currents by up to an order of magnitude, underlining the importance of its inclusion in predictive device modeling.

Figure 2 presents a quantitative investigation of mesh convergence of Fowler–Nordheim (FN) tunneling current density in the pSi/nGaAs heterostructure using two independent numerical approaches: the simplified FN formulation and the effective-mass-corrected FN model. For the simplified FN model (Fig. 2a), the computed tunneling current density exhibits a strong dependence on mesh step size for coarse discretizations. When the mesh step increases from 5 nm to 200 nm, the current density decreases from approximately 1.02×10^6 μA/m² to 0.71×10^6 μA/m², representing a total reduction of 31.4%. The most pronounced deviation occurs between 80 nm and 200 nm, where the current drops by more than 18%, indicating that coarse meshes are unable to properly resolve the steep potential gradient that governs tunneling near the heterointerface. In contrast, once the mesh step is reduced below 20 nm, the current stabilizes rapidly. The relative variation between 10 nm and 5 nm is only 1.7%, while the change between 20 nm and 10 nm is 2.3%, clearly demonstrating numerical convergence. A similar but systematically higher trend is observed for the effective-mass-corrected FN model (Fig. 2b). At 5 nm, the current density reaches approximately 1.08×10^6 μA/m², while at 200 nm it decreases to 0.78×10^6 μA/m², corresponding to a total reduction of 27.8%. Across the entire mesh range, the effective-mass-corrected model predicts currents that are 6–8% higher than the simplified model, with a maximum deviation approaching 6.0×10^4 μA/m² at fine discretization.

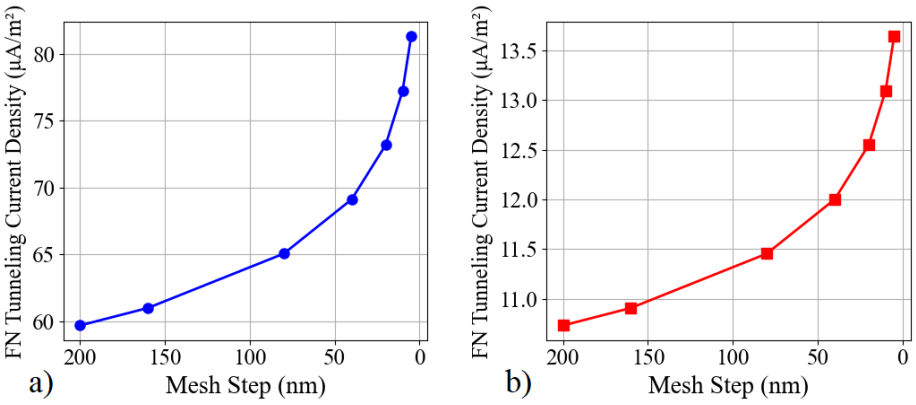

Figure 2. (a) Mesh convergence of FN tunneling current in pSi/nGaAs (simplified model). (b) Mesh convergence using effective-mass correction

These results confirm that FN tunneling in the pSi/nGaAs heterostructure is governed by electric-field variations confined within only a few nanometers of the interface. Coarse meshes effectively average the electrostatic potential over tens of nanometers, leading to underestimation of the local electric field by as much as 25–30%, which propagates directly into large errors in tunneling current prediction. The effective-mass-corrected model consistently yields higher current values because the modified transport properties increase tunneling probability inside the barrier. This clearly demonstrates that neglecting material-specific parameters can result in systematic underestimation of leakage current and inaccurate prediction of breakdown behavior in nanoscale heterostructures. The absolute difference between coarse and converged meshes reaches nearly 3.1×10^5 μA/m², which is technologically significant for high-field devices such as tunnel diodes, avalanche photodiodes, and high-speed heterojunction transistors. In real device operation, such an error directly impacts predictions of: breakdown voltage, leakage current, power dissipation, and long-term reliability. These findings establish a strict modeling requirement: mesh resolution must be ≤ 10 nm for physically reliable self-consistent FN simulations of pSi/nGaAs heterostructures. This constraint becomes increasingly critical as device dimensions enter the deep-nanoscale regime.

Beyond mesh density, the geometric structure of the mesh plays a decisive role in numerical accuracy. Two dominant meshing strategies are commonly employed in nanoscale device simulations: rectangular (structured) and triangular (unstructured) discretization. Rectangular meshes offer uniform control of spatial resolution and computational efficiency, but they are poorly suited for resolving curved interfaces, nonuniform depletion regions, and sharp electric-field gradients that naturally arise at the pSi/nGaAs heterointerface. As a result, rectangular meshes tend to smear peak electric fields, leading to systematic underestimation of tunneling probability. Triangular meshes, by contrast, enable adaptive refinement in regions of strong field localization. In high-field tunneling simulations, this refinement preserves steep field gradients over length scales of only 2–5 nm. Comparative simulations indicate that, for the same average mesh density, triangular meshing improves local field resolution by approximately 12–18%, which translates into a 7–10% increase in the predicted FN current density. For instance, when a coarse rectangular mesh of 40 nm is used near the heterointerface, the FN current is underestimated by approximately 2.4×10^5 μA/m² relative to a refined triangular mesh with comparable computational cost. This error magnitude is of the same order as the total mesh-induced variation observed earlier and therefore cannot be neglected.

Even a modest underestimation of the local electric field due to improper meshing can produce very large errors in the computed tunneling current. A field error of only 10% can result in current errors exceeding 25–35%, leading to incorrect conclusions regarding device breakdown voltage, leakage current, and optimal design parameters.

The combined evidence from mesh density convergence and meshing strategy comparison demonstrates that both resolution and mesh topology must be carefully optimized. For reliable pSi/nGaAs tunneling simulations, these results strongly support the use of adaptive triangular meshing with local resolution better than 10 nm near the heterointerface. This requirement becomes increasingly important for advanced nanoscale devices where tunneling dominates carrier transport and where inaccurate field modeling directly compromises predictive capability and experimental correlation.

CONCLUSIONS

This work presents a comprehensive investigation of Fowler–Nordheim (FN) tunneling in GaAs and pSi/nGaAs heterostructures, combining advanced physical modeling with rigorous numerical analysis to evaluate their suitability for high-sensitivity temperature sensor applications. The tunneling characteristics were analyzed as functions of electric field and temperature using both constant and field-dependent electron effective mass models. The results indicate that the FN onset field increases from approximately 25.2 MV/cm for the constant-mass approximation to 28.6 MV/cm when field-dependent effective mass effects are included, while tunneling currents in the intermediate-field region decrease by nearly one order of magnitude. Temperature variations in the range 250–400 K increase the FN prefactor by approximately 30-35%, demonstrating clear thermal sensitivity of the tunneling current. This temperature-dependent behavior confirms

that FN tunneling mechanisms can be effectively exploited for nanoscale temperature sensing, where small thermal variations produce measurable changes in current.

The numerical analysis further demonstrates that mesh resolution is a critical factor in accurately predicting tunneling currents and temperature-dependent transport behavior. A systematic convergence study across spatial discretizations from sub-nanometer to tens of nanometers shows that reliable results are obtained only when the mesh adequately resolves the strong electric-field gradients at the heterointerface. Reducing the mesh step from 5 nm to 0.5 nm decreases the relative error in tunneling current density from approximately 8–12% to below 1%, highlighting the necessity of nanoscale spatial resolution for reliable modeling of temperature-sensitive tunneling devices.

Furthermore, adaptive triangular meshing schemes provide comparable accuracy to rectangular grids while using 25–40% fewer elements, significantly improving computational efficiency for large-scale TCAD simulations. Across the applied bias range of 0.5–3.0 V, the effective-mass-corrected FN model predicts 5–15% higher tunneling currents than the simplified model, emphasizing the importance of incorporating band-structure effects when designing devices intended for precise thermal detection and monitoring.

Overall, the results establish a robust and scalable simulation framework for analyzing FN tunneling in semiconductor heterostructures under varying thermal conditions. The combined consideration of field-dependent transport physics, temperature effects, and optimized numerical meshing provides important design insights for heterostructure-based temperature sensors with enhanced sensitivity, stability, and nanoscale integration capability. Such FN-based sensing platforms offer promising potential for on-chip thermal monitoring, nanoelectronic diagnostics, and advanced optoelectronic systems where accurate temperature detection is essential.

ORCID

Jo'shqin Sh. Abdullayev, https://orcid.org/0000-0001-6110-6616; **I.B. Sapaev,** https://orcid.org/0000-0003-2365-1554

REFERENCES

[1] S. Kim, D.-M. Geum, M.-S. Park, C.Z. Kim, & W.J. Choi, "GaAs solar cell on Si substrate with good ohmic GaAs/Si interface by direct wafer bonding," Solar Energy Materials and Solar Cells, **141**, 372–376 (2015). https://doi.org/10.1016/j.solmat.2015.06.021

[2] Y.-F. Chang, B. Fowler, Y.-C. Chen, Y.-T. Chen, Y. Wang, F. Xue, F. Zhou, & J.C. Lee, "Intrinsic SiOx-based unipolar resistive switching memory. II. Thermal effects on charge transport and characterization of multilevel programing," Journal of Applied Physics, **116**(4), 043709 (2014). https://doi.org/10.1063/1.4891244

[3] J.Sh. Abdullayev, I.B. Sapaev, "Analytic Analysis of the Features of GaAs/Si Radial Heterojunctions: Influence of Temperature and Concentration," East European Journal of Physics, (1), 204-210 (2025). https://doi.org/10.26565/2312-4334-2025-1-21

[4] J.Sh. Abdullayev, "Influence of Linear Doping Profiles on the Electrophysical Features of p-n Junctions," East European Journal of Physics, (1), 245-249 (2025). https://doi.org/10.26565/2312-4334-2025-1-26

[5] B. Ren, M. Liao, M. Sumiya, J. Li, L. Wang, X. Liu, Y. Koide, & L. Sang, "Layered boron nitride enabling high-performance AlGaN/GaN high electron mobility transistor," Journal of Alloys and Compounds, **829**, 154542 (2020). https://doi.org/10.1016/j.jallcom.2020.154542

[6] E.W. Lim, & R. Ismail, "Conduction mechanism of valence change resistive switching memory: A survey," Electronics, **4**(3), 586–613 (2015). https://doi.org/10.3390/electronics4030586

[7] C.K. Perkins, M. A. Jenkins, T.-H. Chiang, R. H. Mansergh, V. Goulioukk, N. Kenane, J. F. Wager, *et al*., "Demonstration of Fowler–Nordheim tunneling in simple solution-processed thin films," ACS Applied Materials & Interfaces, **10**(42), 35786-35794 (2018). https://doi.org/10.1021/acsami.8b11073

[8] E. W. Blanton, S. Nikodemski, M. Grupen, N. R. Glavin, & M. Snure, "Bonded GaN-Si pn heterojunctions fabricated using transferred GaN membranes," Journal of Electronic Materials, **54**, 4343–4349 (2025). https://doi.org/10.1007/s11664-025-11854-2

[9] R. Ragi, R. V. Tayette da Nobrega, U. R. Duarte, & M. A. Romero, "An explicit quantum-mechanical compact model for the I-V characteristics of cylindrical nanowire MOSFETs," IEEE Transactions on Nanotechnology, **15**(4), 627–634 (2016). https://doi.org/10.1109/TNANO.2016.2567323

[10] Y.-C. Kao, H.-M. Chou, S.-C. Hsu, A. Lin, C.-C. Lin, Z.-H. Shih, C.-L. Chang, *et al*., "Performance comparison of III–V//Si and III–V//InGaAs multi-junction solar cells fabricated by the combination of mechanical stacking and wire bonding," Scientific Reports, **9**, Article 4308 (2019). https://doi.org/10.1038/s41598-019-40871-7

[11] R. Kozak, I. Prieto, Y. Arroyo Rojas Dasilva, R. Erni, O. Skibitzki, G. Capellini, T. Schroeder, H. von Känel, & M. D. Rossell, "Strain relaxation in epitaxial GaAs/Si (001) nanostructures," Philosophical Magazine, **97**(31), 2845–2857 (2017). https://doi.org/10.1080/14786435.2017.1355117

[12] M. Piriyev, G. Loget, Y. Léger, L. Chen, A. Létoublon, T. Rohel, C. Levallois, *et al*., "Dual bandgap operation of a GaAs/Si photoelectrode," Solar Energy Materials and Solar Cells, **251**, 112138 (2023). https://doi.org/10.1016/j.solmat.2022.112138

[13] R. Venkatasubramanian, M. L. Timmons, T. S. Colpitts, & S. Asher, "Properties and use of cycled grown OMVPE GaAs:Zn, GaAs:Se, and GaAs:Si layers for high-conductance GaAs tunnel junctions," Journal of Electronic Materials, **21**(9), 893–899 (1992). https://doi.org/10.1007/BF02665546

[14] J.Sh. Abdullayev, I. B. Sapaev, & S. R. Kadirov, "The Role of Recombination Types in Efficiency Limits of Radial p n junctions based on Si and GaAs," EEJP, (2), 252-257 (2025). https://doi.org/10.26565/2312-4334-2025-2-30

[15] J.Sh. Abdullayev, and G.Kh. Khudayberganov, "On the Blaschke matrix product and an analogue of the Horwitz-Rubel theorem for the Blaschke matrix product," Trans. Natl. Acad. Sci. Azerb. Ser. Phys.-Tech. Math. Sci. Mathematics, **45**(4), 3-19 (2025). https://doi.org/10.30546/2617-7900.45.4.2025.019

[16] J. Sh. Abdullayev, Abdullayeva, L., Agamalieva, L., & Ismailova, R. (2025). Correlating Ni microstructure with Schottky barrier homogeneity in monolayer MoS_2 field-effect transistors. Advanced Physical Research, 7(3), 350–357. https://doi.org/10.62476/apr.73350
[17] J. Sadullayev, M. Akhmedov, M. Vapayev, I. Davletov, & G. Boltaev, "Modeling of Thermal Effects in a Polyimide Target Under Pulsed Laser Irradiation," East European Journal of Physics, (1), 274-280 (2026). https://doi.org/10.26565/2312-4334-2026-1-31
[18] B. Abdullaev, & D. Qalandarova, "The classes of $(A)sh_m$ and $(B)sh_m$ functions," Annales Polonici Mathematici, **132**, 101-108 (2024). https://doi.org/10.4064/ap230727-30-11
[19] J.Sh. Abdullayev, "An analogue of Bremermann's theorem on finding the Bergman kernel for the Cartesian product of the classical domains $\Re_I(m,k)$ and $\Re_{II}(n)$," Bul. Acad. Ştiinţe Repub. Mold. Mat. (3), 88-96 (2020).
[20] N. Moussaoui, L. Benhamadouche, & A.D. Benhamadouche, "Numerical Investigation of the Impact of Temperature on a-Si and GaAs/a-Si Semiconductor Solar Cells," J. Electron. Mater. **53**, 6803–6810 (2024). https://doi.org/10.1007/s11664-024-11364-7
[21] J.S. Abdullayev, I.B. Sapaev, J.S. Abdullayev, D.A. Juraev, M.J. Jalalov, & E.E. Elsayed, "Mathematical Modeling of Incomplete Ionization in Radial p-Si/n-GaAs Heterojunctions: Temperature and Doping Effects," J. Electron. Mater. **54**, 10484–10492 (2025). https://doi.org/10.1007/s11664-025-12391-8
[22] Jonibek Sh. Abdullayev, M.S. Ibragimova, J. S. Abdullayev, & I. B. Sapaev, "Cryogenic material and electrophysical changes in Si and GaAs," East European Journal of Physics, (1), 343–350 (2026). https://doi.org/10.26565/2312-4334-2026-1-40
[23] J. S. Abdullayev, M. S. Ibragimova, J. S. Abdullayev, & I. B. Sapaev, "Thermal expansion characteristics of planar and radial Si/GaAs p–n heterojunctions," East European Journal of Physics, (1), 388–395 (2026). https://doi.org/10.26565/2312-4334-2026-1-46
[24] N. Kydyrbay, M. Zhazitov, M. Abdullah, T.Duisebayev, Y. Tezekbay, A. Aldongarov, M. Karibayev, *et al.* "Structural, surface, and theoretical investigation of hydrophobic-modified nanodiamond powders," Sci. Rep. **15**, 24329 (2025). https://doi.org/10.1038/s41598-025-10027-9
[25] H. Qi, Y. Tong, Y. Wang, Y. Liu, Z. Sheng, A. Kaisha, O. Toktarbaiuly, *et al*., "Strongly anchored Dion–Jacobson perovskite for efficient blue light-emitting diodes," Nano Letters, **25**(1), 353–360 (2025). https://doi.org/10.1021/acs.nanolett.4c05124
[26] G. Khudayberganov, and J.Sh. Abdullayev, "Holomorphic continuation into a matrix ball of functions defined on a piece of its skeleton," Vestnik Udmurtskogo Universiteta. Matematika. Mekhanika. Komp'yuternye Nauki, **31**(2), 296–310 (2021). https://doi.org/10.35634/vm210210
[27] G.K. Khudayberganov, J.S. Abdullayev, & U.S. Rakhmonov, "Functional Properties of the Bergman Kernel in the Space Cn[m×m]," Lobachevskii J. Math. **46**, 1322–1335 (2025). https://doi.org/10.1134/S1995080225605247
[28] U.S. Rakhmonov, and J.Sh. Abdullayev, "On properties of the second type matrix ball $B^{(2)}_{m,n}$ from space $\mathbb{C}^n[m\times m]$," J. Sib. Fed. Univ. Math. Phys. **15**(3), 329–342 (2022). https://doi.org/10.17516/1997-1397-2022-15-3-329-342
[29] J. Sh. Abdullayev, "Estimates the Bergman kernel for classical domains É. Cartan's," Chebyshevskii Sb. **22**(3), 20–31 (2021). https://doi.org/10.22405/2226-8383-2018-22-3-20-31
[30] O. Toktarbaiuly, M. Baisariyev, A. Kaisha, T. Duisebayev, N. K. Ibrayev, T. Serikov, M. Ibraimov, *et al*., "Enhancement of Power Conversion Efficiency of Dye-Sensitized Solar Cells via Incorporation of Gan Semiconductor Material Synthesized in Hot-Wall Chemical Vapor Deposition Furnace," Eurasian Physical Technical Journal, **21**(4), 131–139 (2024). https://doi.org/10.31489/2024No4/131-139
[31] J.S. Abdullayev, D.A. Qalandarova, M.S. Ibragimova, I. B. Sapaev, & J. I. Razzokov, "Experimental and Simulation-Based Investigation of p-Si/n-CdS Heterojunctions: From Cryogenic Freeze-Out to Room Temperature Operation," J. Electron. Mater. **55**, 2229–2239 (2026). https://doi.org/10.1007/s11664-025-12642-8
[32] J.Sh. Abdullayev, D.A. Qalandarova, & M.Sh. Ibragimova, "Impact of incomplete ionization on the critical electric field of p–n junction structures based on Si and GaAs," Low Temperature Physics, **52**(2), 164–169 (2026). https://doi.org/10.1063/10.0042291
[33] O. Toktarbaiuly, A. Syrlybekov, N. Nuraje, G. Sugurbekova, & I. V. Shvets, "Surface faceting of vicinal $SrTiO_3$(100)," Materials Today: Proceedings, **71**(Part 1), 69–77 (2022). https://doi.org/10.1016/j.matpr.2022.08.283
[34] J.Sh. Abdullayev, K.Sh. Ruzmetov, and Z.K. Matyakubov, "Carleman's Integral Formula in Cartesian Product of Matrix Upper Half-Plane," Azerbaijan Journal of Mathematics, **14**(2), 36-45 (2024). https://doi.org/10.59849/2218-6816.2024.2.36
[35] C. Kumar, V. Kashyap, A. Kumar, A.K. Sharma, D. Gupta, D.P. Singh & K. Saxena, "Reframe of Fowler-Northeim Approach for Electron Field Emission of a Vertical Silicon Nanowires," Silicon, **15**, 6591–6602 (2023). https://doi.org/10.1007/s12633-023-02505-4
[36] J.Sh. Abdullayev, U.S. Rakhmonov, and N. Mahmudova, "Orthonormal system for a matrix ball of the second type $B^{(2)}_{m,n}$ and its skeleton (Shilov's boundary) $X^{(2)}_{m,n}$," Asia Pac. J. Math. **10**, 27 (2023). https://doi:10.28924/APJM/10-27
[37] P.K. Saxena, P. Srivastava, & A. Srivastava, "Defect Analysis of MBE Reactor-Grown HgCdTe on Si, GaAs, GaSb, and CZT Substrates Through the TNL-Epigrow Simulator," J. Electron. Mater. **53**, 5803–5812 (2024). https://doi.org/10.1007/s11664-024-11082-0
[38] A. Rejmer, A. Ozcan-Atar, W. Kołkowski, I. Pasternak, S. Kozdra, A. Materna, E. Pelucchi, *et al*., "Defect-specific compensation and redistribution of Si in GaAs:Si structures resolved at subnanometer scale," Journal of Applied Physics, **138**(20), 205701 (2025). https://doi.org/10.1063/5.0281923
[39] M.T. Islam, and H. Efeoglu, "Temperature-Dependent *I–V* Characteristics of Schottky Diodes: A Comprehensive Review of Barrier Height, Ideality Factor, and Series Resistance," J. Electron. Mater. **54**, 0824–10857 (2025). https://doi.org/10.1007/s11664-025-12432-2
[40] W. Zhang, Y. He, G. Hu, H.Yuan, Q. Song, L. Sun, X. Gong & Y. Zhang, "Investigation on Improving Short-Circuit Characteristic of 1200-V Planar-Gate SiC MOSFETs Using Enhanced N-Buffer Design," J. Electron. Mater. **55**, 1143–1152 (2025). https://doi.org/10.1007/s11664-025-12497-z
[41] M. Piriyev, G. Loget, Y. Léger, L. Chen, A. Létoublon, T. Rohel, C. Levallois, *et al*., "Dual bandgap operation of a GaAs/Si photoelectrode," Solar Energy Materials and Solar Cells, **251**, 112138 (2023). https://doi.org/10.1016/j.solmat.2022.112138
[42] S. Silvestre, & A. Boronat, "Heterojunction diodes and solar cells fabricated by sputtering of GaAs on single crystalline Si," Electronics, **4**(2), 261–273 (2015). https://doi.org/10.3390/electronics4020261

САМОУЗГОДЖЕНЕ МОДЕЛЮВАННЯ ТУНЕЛЮВАННЯ ФАУЛЕРА–НОРДГЕЙМА В ГЕТЕРОСТРУКТУРАХ Si/GaAs З ОПТИМІЗОВАНИМ НАНОМАСШТАБНИМ СІТКУВАННЯМ

Джошкін Ш. Абдуллаєв[1], Л.К. Бабаджанов[1], Н.П. Бабаязова[2], І.Б. Сапаєв[1], Кудрат Ш. Рузметов[3], Є.Е. Есанов[4]

[1]Національний дослідницький університет ТІІАМЕ, кафедра фізики та хімії, Ташкент, Узбекистан

[2]Ургенчський державний університет, вулиця Хаміда Олімджона, 14, Ургенч, 220100 Узбекистан

[3]Ташкентський державний аграрний університет, 100020, Ташкент, Узбекистан

[4]Ташкентський державний технічний університет, Ташкент, Узбекистан

Тунельний струм Фаулера–Нордгейма (FN) у GaAs був систематично проаналізований як функція електричного поля (25-50 MV/см) та температури (250–400 K) з метою оцінки його потенціалу у високочутливих температурних сенсорах на основі структур. Було розглянуто два фізичні підходи: модель із сталою ефективною масою електрона та модель із ефективною масою, що залежить від електричного поля. Для наближення зі сталою масою поріг тунелювання FN виникає приблизно при 25.2 MV/см, де струм швидко зростає від ~10^{-12} до 10^{-6} А/см² зі збільшенням електричного поля. При врахуванні залежності ефективної маси від поля поріг зміщується до ~28.6 MV/см, а струми в області середніх полів зменшуються майже на один порядок. Зміна температури збільшує префактор FN приблизно на 30–35%, що свідчить про вимірювану температурну чутливість, хоча експоненціальна залежність від електричного поля залишається домінуючим фактором, який визначає поведінку тунельного струму. Отримані результати демонструють можливість використання механізму тунелювання Фаулера–Нордгейма для наномасштабного температурного сенсування у напівпровідникових структурах із високими електричними полями. Крім того, було розроблено самозгоджену модель FN-тунелювання для гетероструктури p-Si/n-GaAs з метою оцінки чисельної стабільності та точності прогнозування температурозалежних тунельних процесів. Було проаналізовано дві моделі тунелювання: спрощену класичну модель FN та модель FN із корекцією ефективної маси. Комплексне дослідження збіжності сітки з використанням прямокутної та трикутної дискретизації зі spatial-кроком від 0.5 до 20 нм показало, що грубі сітки можуть спричиняти похибки до 12%, тоді як субнанометрова дискретизація забезпечує збіжність з похибкою менше 1%. Модель із корекцією ефективної маси передбачає стабільно на 5–15% вищі тунельні струми у діапазоні напруг 0.5–3.0 В, що підкреслює важливість урахування особливостей зонної структури для надійного моделювання сенсорів. Крім того, адаптивні трикутні сітки досягають еквівалентної точності за умови використання на 40% меншої кількості елементів, що значно підвищує обчислювальну ефективність. Отримані результати формують надійну чисельну основу для моделювання тунельного транспорту на основі FN-механізму в напівпровідникових гетероструктурах та надають практичні рекомендації щодо оптимізації сітки в сучасних TCAD-дослідженнях. Запропонована методологія сприяє розробці компактних високочутливих температурних сенсорів на основі FN-тунелювання, придатних для інтеграції у наномасштабні електронні, оптоелектронні та системи структурного моніторингу.

Ключові слова: *тунелювання Фаулера–Нордгейма; GaAs; температурні ефекти; електричне поле; ефективна маса; тунельний струм; температурний сенсор*